

Characterization of the room temperature payload prototype for the cryogenic interferometric gravitational wave detector KAGRA

Fabián Erasmo Peña Arellano,^{1,a)} Takanori Sekiguchi,² Yoshinori Fujii,¹ Ryutaro Takahashi,¹ Mark Barton,¹ Naoatsu Hirata,¹ Ayaka Shoda,¹ Joris van Heijningen,³ Raffaele Flaminio,¹ Riccardo DeSalvo,^{4,5} Koki Okutumi,⁶ Tomotada Akutsu,¹ Yoichi Aso,¹ Hideharu Ishizaki,¹ Naoko Ohishi,¹ Kazuhiro Yamamoto,² Takashi Uchiyama,² Osamu Miyakawa,² Masahiro Kamiizumi,² Akiteru Takamori,⁷ Ettore Majorana,⁸ Kazuhiro Agatsuma,³ Eric Hennes,³ Jo van den Brand,³ and Alessandro Bertolini³

¹National Astronomical Observatory of Japan, 2-21-1 Osawa, Mitaka-shi, Tokyo 181-8588, Japan

²Institute for Cosmic Ray Research, 5-1-5 Kashiwanoha, Kashiwa-shi, Chiba 277-8582, Japan

³National Institute for Subatomic Physics, Nikhef Science Park 105, 1098 XG Amsterdam, The Netherlands

⁴Waves Group, University of Sannio at Benevento, Benevento I-82100, Italy

⁵California State University Los Angeles, 5151 State University Drive, Los Angeles, California 90032, USA

⁶SOKENDAI, The Graduate University for Advanced Studies, Shonan Village, Hayama,

Kanagawa 240-0193, Japan

⁷Earthquake Research Institute, University of Tokyo, 1-1-1, Yayoi, Bunkyo-ku, Tokyo 113-0032, Japan

⁸Istituto Nazionale di Fisica Nucleare, INFN, P.le A. Moro 2, I-00185 Rome, Italy

(Received 8 December 2015; accepted 12 February 2016; published online 1 March 2016)

KAGRA is a cryogenic interferometric gravitational wave detector currently under construction in the Kamioka mine in Japan. Besides the cryogenic test masses, KAGRA will also rely on room temperature optics which will hang at the bottom of vibration isolation chains. The payload of each chain comprises an optic, a system to align it, and an active feedback system to damp the resonant motion of the suspension itself. This article describes the performance of a payload prototype that was assembled and tested in vacuum at the TAMA300 site at the NAOJ in Mitaka, Tokyo. We describe the mechanical components of the payload prototype and their functionality. A description of the active components of the feedback system and their capabilities is also given. The performance of the active system is illustrated by measuring the quality factors of some of the resonances of the suspension. Finally, the alignment capabilities offered by the payload are reported. © 2016 AIP Publishing LLC. [<http://dx.doi.org/10.1063/1.4942909>]

I. INTRODUCTION

KAGRA (alluding to Kamioka and gravitational wave) is an interferometric gravitational wave detector currently under construction in the Kamioka mine in Japan. Its main target is gravitational waves produced by binary neutron stars at a frequency of around 100 Hz,¹ where the interferometer will be most sensitive. The novel features of this system are that its test masses will be cryogenic in order to reduce thermal noise² and that it will be located underground, where seismic noise and gravity gradient noise are expected to be low.³ In its final configuration, KAGRA will be a Michelson interferometer with high finesse Fabry-Perot cavity arms, with a total of four cryogenic test masses. For the rest of its subsystems, KAGRA will rely on room temperature components. The beam splitter and three signal recycling mirrors will be held by the Type B vibration isolation chain, whereas the optics of the power recycling system will be supported by the Type B_p chain, both of which are briefly described in Sec. II. As part of the development of the Type B system, a prototype was assembled and tested at the TAMA300 site at NAOJ in Tokyo.

This article reports the characterization of the payload of such a prototype.

Besides holding the optic, the payload should provide mechanisms to adjust the orientation of the optic and to damp the oscillations of the different bodies that the payload itself comprises. As in Virgo and TAMA300, alignment control is achieved with an upper marionette⁴ whose orientation can be adjusted by remotely changing the position of its center of mass. The damping of the resonant modes is achieved by actively using displacement sensors and actuators. Such devices are called OSEMs, acronym which stands for optical sensor and electromagnetic actuator, and have been extensively tested in LIGO.⁵ The aim of this paper is to report the alignment capabilities and the amount of damping achieved in the prototype.

Sec. II briefly describes the Type B system with the aim of showing the place of the payload within the isolation chain rather than reporting its performance.^{6,7} Sec. III describes the mechanical configuration of the payload and its design features. In Sec. IV the OSEMs are described. Sec. V reports the values of the quality factor Q of the various resonances of the payload with and without the active control system. Sec. VI describes the measurement of the alignment range of the marionette.

^{a)}Author to whom correspondence should be addressed. Electronic mail: fabian.arellano@nao.ac.jp

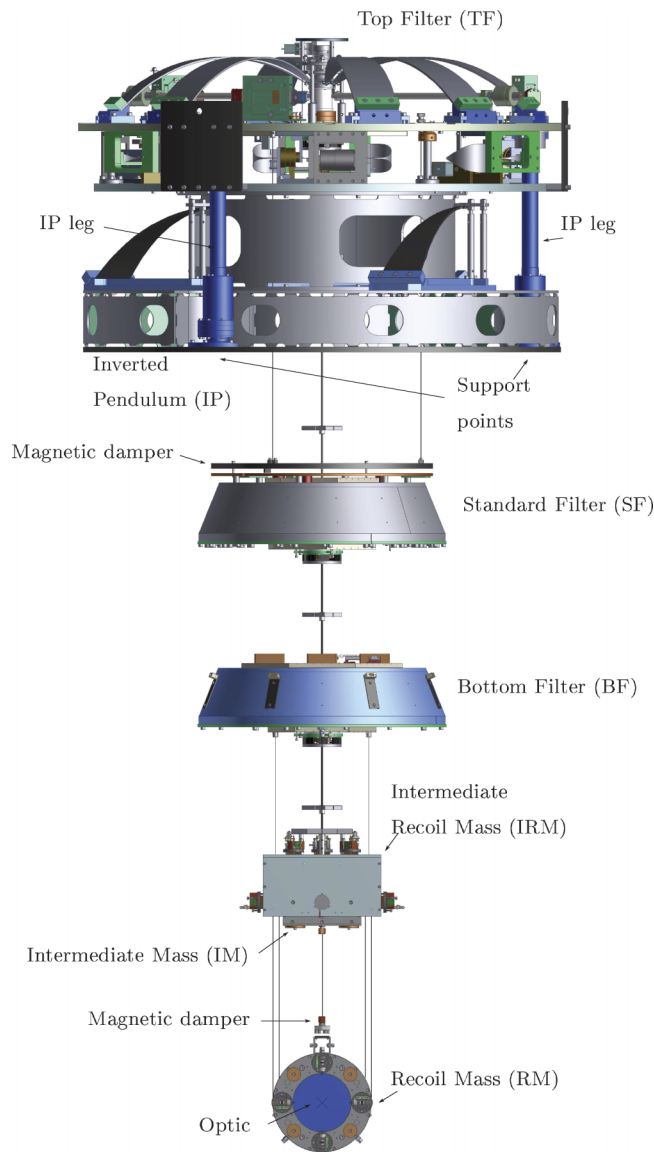


FIG. 1. Type B seismic isolation system.

II. BRIEF DESCRIPTION OF TYPE B VIBRATION ISOLATION SYSTEM

Fig. 1 shows a model of the Type B isolation chain. The uppermost stage is a pre-isolator comprising an inverted pendulum (IP) table⁸ supporting a large diameter vertical geometric anti-spring (GAS) Top Filter⁹ (TF). Its resonant frequency is tuned to about 0.1 Hz. The IP aims to damp the microseismic motion at about 0.2 Hz and any vibration which may excite any pendulum mode of the whole chain above that frequency. From the top filter keystone, a smaller vertical GAS filter, which is called Standard Filter (SF), hangs from a central maraging steel rod. A cap allows the filter to be suspended at its center of mass and provides support to an aluminium ring used for damping the yaw resonant modes of the chain with eddy currents. The magnetic element of the damper hangs from the top filter with three maraging wires. The resonant frequency of the SF is tuned to about 0.3 Hz. Below the SF, another GAS filter hangs, which is called the Bottom Filter (BF). As will be pointed out in Secs. III and V, besides filtering vertical

vibrations, it also aids in the alignment of the payload, which comprises all the components that hang from it.

The Type B_p system is a simplified version of the Type B. It comprises the SF, BF, the payload, and a device called a traverser, which is used for adjusting the position of the SF in the horizontal plane.

III. DESCRIPTION OF THE PAYLOAD

Fig. 2 shows the payload. The upper bodies are the Intermediate Recoil Mass (IRM) and the Intermediate Mass (IM).

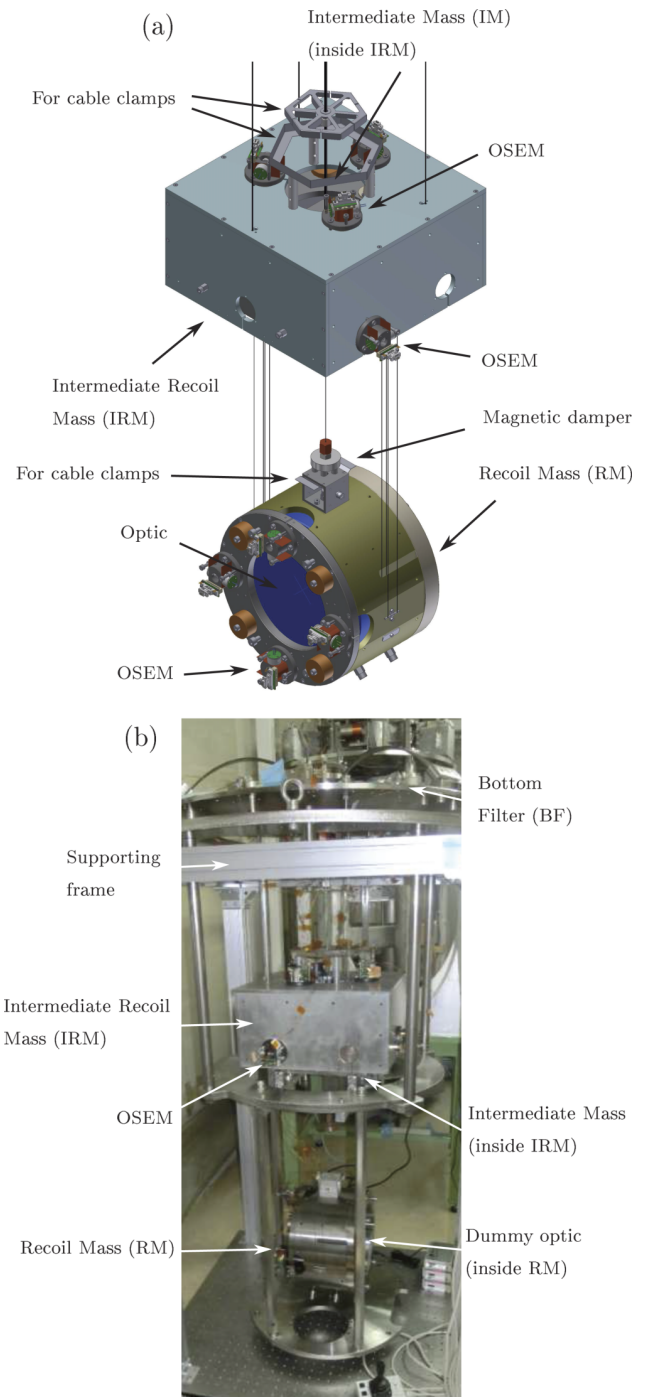


FIG. 2. (a) The payload comprises an intermediate and a bottom assembly. (b) Picture of the payload.

The IRM covers the IM almost completely and therefore the latter is not visible in the drawing. The IM works as a marionette for the optic. The IM and the IRM hang from the BF independently of each other. The lower bodies are the optic and a surrounding concentric Recoil Mass (RM). In a similar fashion to the IM and the IRM, they hang from the IM independently of each other. The function of the IRM and the RM is to hold the active components of the control system, which are called OSEMs. As will be explained in Sec. IV, each OSEM is an assembly of a shadow displacement sensor and a coil-magnet actuator.

Fig. 3(a) shows a drawing of the IM. It is an aluminium box partitioned into upper and lower sections and $23 \times 23 \times 15$ cm in size. Its mass is 26.5 kg including the ballast weight. In the drawing, the suspension rod, the wire clamps for the optic and the RM, the OSEM flags, and the inserts for locking the IRM to the IM are clearly seen. Fig. 3(b) shows the upper cavity of the IM. It houses a mechanism for adjusting the tilt of the IM in roll. The mechanism comprises a stainless steel body of 879 g that can move back and forth under the action of a piezoelectrically actuated micrometer (in red) and a spring pressing the body against the micrometer. As shown, the moving body has a hole for the suspension rod (visible in Fig. 3(a)) to go through. The lower cavity houses a similar mechanism for adjusting the tilt of the IM in pitch. Both cavities host ballast weights that are not shown in the drawing for clarity. In the prototype, both moving stainless steel

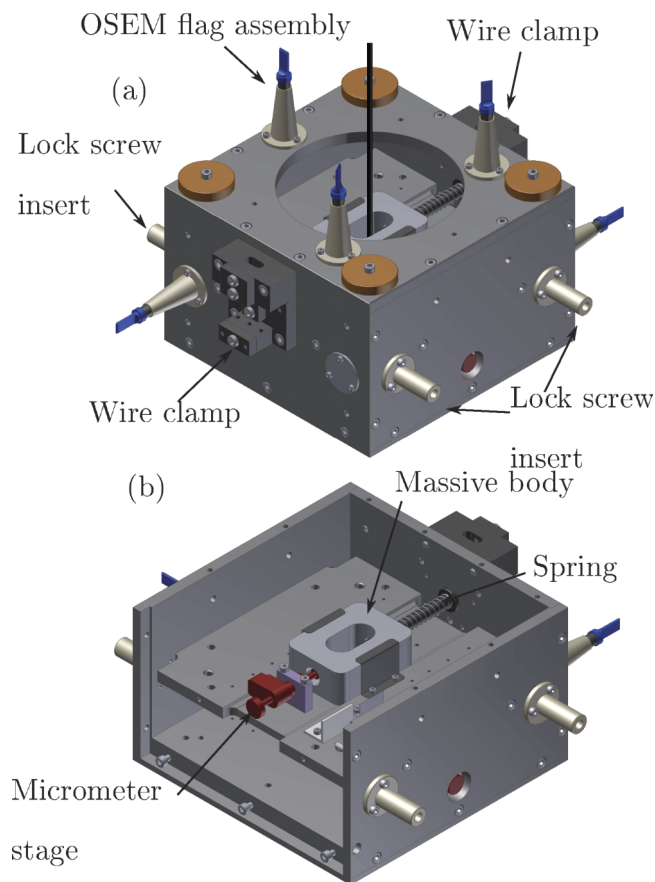


FIG. 3. The intermediate mass works as a marionette for the mirror. A system of moving bodies is used to adjust its tilt in roll and pitch.

bodies lie directly on aluminium surfaces. In the first attempt to align the IM, it became apparent that the static friction was keeping the bodies from moving despite the force exerted by the springs when the picomotor retracted. The solution was to apply UHV compatible lubricant to surfaces in contact. This was an acceptable strategy for the prototype since it was not a clean experiment and because the vacuum was going to be relatively low (below 3 Pa). However, in the KAGRA payload, these bodies will slide on PEEK (polyether ether ketone) rails.

The capabilities of this alignment system were calculated¹⁰ assuming that the effective suspension point of the IM from the BF is above its center of mass by 1 mm. Although the clamping points at the optic and RM are at the same height as their respective centers of mass, the stiffness of the wires (200 μm piano wire for the optic and 600 μm tungsten wire for the RM) places the effective suspension points higher. Upon tilt, this in turn produces a displacement of the centers of mass sideways, away from the position in which the torques are null. The amount of the tilt is, therefore, determined by the compromise between the torques produced by the moving bodies within the IM, the IM itself, the suspension wires, the optic, and the RM. The torques produced by the wires were taken into account by considering their effective bending lengths. Since the traveling range of the micrometer is 25.4 mm full span, the system is designed to provide roll and pitch adjustment of $\pm 2.5^\circ$ maximum. However, as will be reported in Sec. VI, the alignment range is limited by the space in which the OSEM flags can move without touching the OSEM bodies, which is smaller.

Fig. 4(a) shows a cross section of the IM. At the center, coming from above, the suspension rod is clearly seen. As it approaches the clamping point, the thickness changes from 4.5 mm to 2 mm. The thicker section eases the manufacture whereas the thinner sections close to the nail heads aim to reduce the bending length. The nominal position of the center of mass of the IM is marked with a cross and a horizontal line is drawn to illustrate that the OSEM flags on the sides of the IM (only one of three is shown) are at the same height. Fig. 4(b) shows a close up of the region within the rectangle. It is the mechanism used to hang the IM from the BF. This device also provides the means to adjust the position of the effective suspension point with respect to the center of mass. The suspension rod has a cylindrical nail head that hooks into a piece whose lower section is threaded. This piece is screwed from the inside into a threaded hole at the floor of the IM. By adjusting the height of this hook, it is then possible to adjust the position of the effective suspension point. During alignment, the height was adjusted by tuning the pitch frequency of the payload by visual inspection to a value which was later measured to be 0.343 Hz. In these conditions, the center of mass of the IM is close below the effective suspension point but not too close to compromise stability. Fig. 4(c) shows a detail of the hook. Inside the cavity, there is a nominal gap of 50 μm plus manufacturing tolerances around the nail head to the inner surface of the hook. This design aims to produce a purely compressive attachment, free of shear stress.

Fig. 2 shows a drawing of the IRM which extends around the IM. Its function is to hold six OSEMs that are used to control the IM. It is made mostly of aluminium and its mass

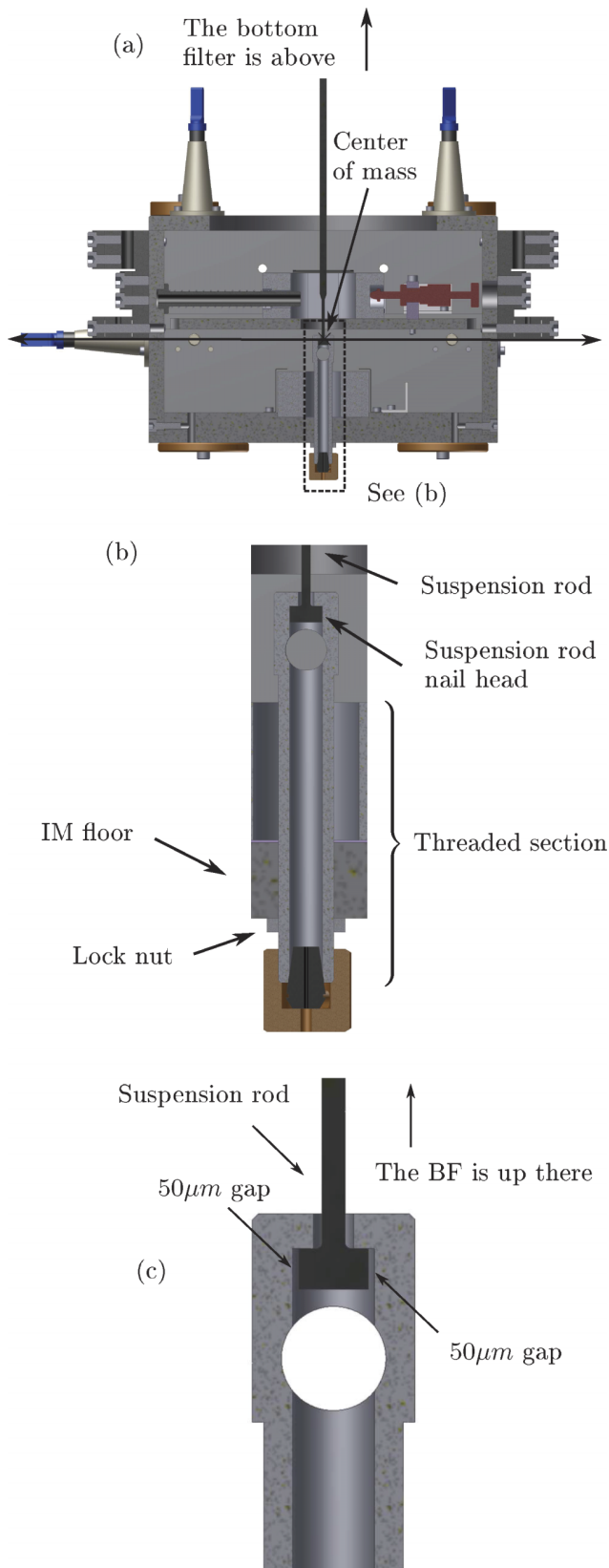


FIG. 4. (a) Cross section view of the IM. (b) Cross section view of the suspension rod hook (c) Detail of top section of (b).

is 8.14 kg including the OSEMs. The IRM hangs from the BF with three 2 mm thick maraging steel rods. The aim of such a rigid suspension for a relatively light body is to provide a strong authority over the IM. The authority is further enhanced

by the inertia of the BF, whose mass is about 115 kg. Due to the stiffness of this mechanical link and the position of the clamping points, successful alignment of the payload requires the adjustment of the orientation of the BF. This is achieved by moving a set of four massive bodies supported on its cap using motorized micrometers working in conjunction with springs.

At the very bottom, the optic and the RM hang. In the prototype, a dummy optic consisting of an aluminium cylinder with a size and a weight similar to one of the real KAGRA power recycler mirrors was used. It has a diameter of 250 mm, a thickness of 100 mm, and a weight of 10.7 kg. Circular holes were made in the cylinder in order to achieve the desired weight while keeping the center of mass at the geometrical center. The optic hangs from the IM by means of two 200 μm piano wires that loop underneath the optic and whose ends are held by the clamps on the sides of the IM (see Fig. 3(a) where one is shown). The separation between the wires is 10 mm along the cylindrical part of the optic. The meeting point of the wires with the optic is determined by cylindrical wire breakers with grooves to host the wires. The wire breakers are at the same height as the center of mass of the optic and the clamping points at the IM are at the same height as the center of mass of the IM. The nominal length of the wires from the clamping points to the wire breakers is 587 mm. Attached to the optic are the OSEM flags, which will be described in Sec. IV. In the prototype, they are arranged in cross configuration “+” close to the edge of the optic.

The RM surrounds the optic and also hangs from the IM. It is a hollow cylinder made of titanium that, once mounted, is closed at both ends by ring-shaped caps with circular apertures to allow the light through. Titanium was selected because it is non-magnetic, it produces low eddy current dissipation due to its low conductivity, and it is compatible with ultra-high vacuum. The back ring holds four OSEMs. The cylinder and both caps also hold screws with small glass spheres at their tips to work as earthquake stops and for locking the optic for transportation. The RM is supported by two 600 μm tungsten wires that also loop underneath the RM. The separation between these wires is 20 mm front to back and their ends are clamped at the IM at the same clamp assemblies and at the same height as the wires for the optic. The meeting point of the wires with the RM is also determined by grooved cylindrical wire breakers. At the top of the RM, there is a component made of aluminium used as an eddy current damper. The magnetic element of the damper hangs from the IM via a tungsten rod and is intended to reduce the differential modes of oscillation between the IM and the RM.

As part of the development of the Type B system, a numerical rigid body simulation, called SUMCOM,^{6,11,12} was developed. During the assembly, the transfer functions for the various degrees of freedom of the partially assembled system were measured. In the case of the payload, this was achieved using the OSEMs. Namely, for the IM and IRM, those degrees of freedom are longitudinal along the optic axis of the main interferometer, vertical, transverse, pitch, roll, and yaw. For the optic, they are longitudinal along the optic axis, pitch, and yaw. Comparisons with the predictions were used to identify and fix faulty behaviour.¹³ As an example, Fig. 5 shows the transfer function of the IM in yaw. All the transfer functions were

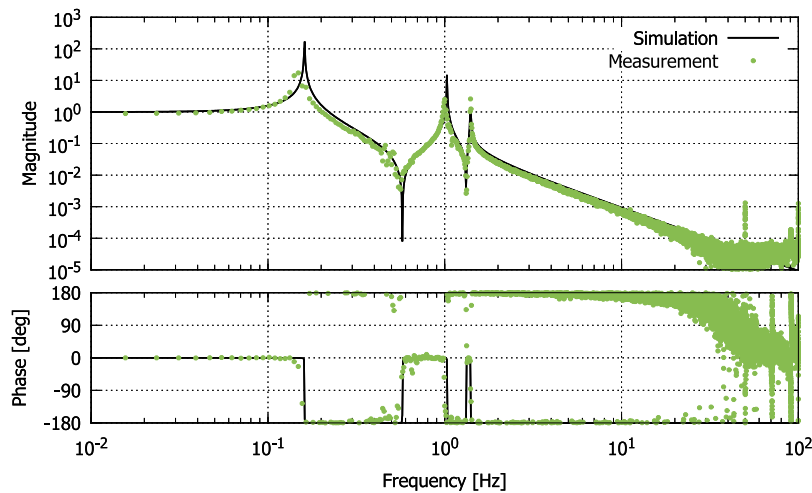


FIG. 5. Transfer function of the IM in yaw.

measured from virtual actuators to virtual sensors after an iterative diagonalization procedure¹⁴ carried out at frequencies between 0.1 Hz and 0.03 Hz, achieving couplings of 1% and less.

IV. LOCAL SENSORS AND ACTUATORS ON THE PAYLOAD

The OSEMs are the position sensors and actuators used to damp the resonances of the payload. OSEM stands for optical sensor and electromagnetic actuator. As Fig. 2 suggests, the whole payload uses ten OSEMs, six mounted on the IRM and four on the RM. At the IM level, they measure three longitudinal and three angular degrees of freedom. At the optic level, they measure the longitudinal degree of freedom along the optic axis, pitch, and yaw. The OSEM combines a simple shadow sensor and a coil-magnet actuator. Figs. 6(a) and 6(b) show two views of the OSEM. The first view shows the LED (Light Emitting Diode) and lens assembly on one side and, on the opposite side, the partially hidden photodiode holder. It also shows the micro-D connector, but the wiring to the LED, photodiode, and coil is not depicted. At the center of the OSEM body, there is a cavity into which the flag, which is attached either to the optic or to the IM, is inserted from behind. Fig. 6(b) shows a cross section of the OSEM. On the left lie the LED and a collimating lens. On the right, there is a photodiode within a can. In between the lens and the photodiode, the flag is inserted. The opposite end of the flag is attached to the optic, which is not shown. The movement of the flag along the Z direction changes the amount of light reaching the photodiode and thus the displacement is quantified. Fig. 6(b) also shows the actuation coil and the magnet within the flag. The flag is designed so that at the nominal position, the tip blocks half the light and the magnet is at the position where the actuation force is the largest.¹⁵ The thickness of the flag is 2 mm and it is inserted into a spacing 5.1 mm wide in between the LED and photodiode holders. The flag becomes narrow at the tip in order to decrease coupling between the linear displacement and tilt of the flag.

The current produced by the photodiode was amplified with a simple transimpedance amplifier, producing a final output in volts. The output was calibrated in terms of displac-

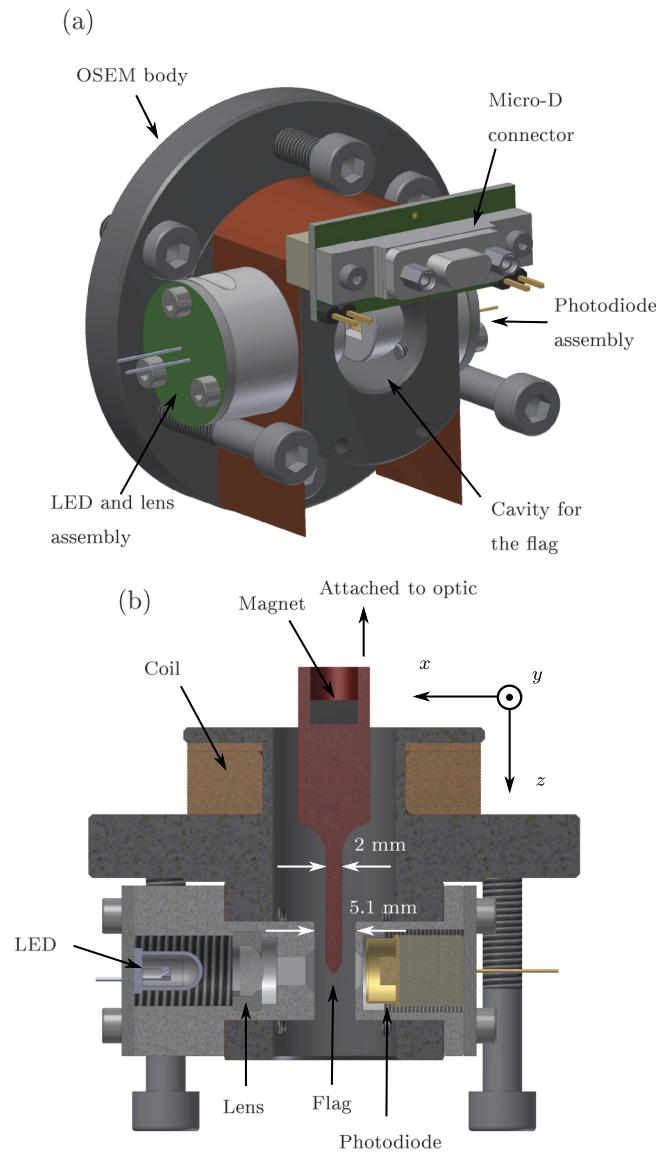


FIG. 6. (a) The OSEM is the active element of the control system. (b) A cross section view of an OSEM.

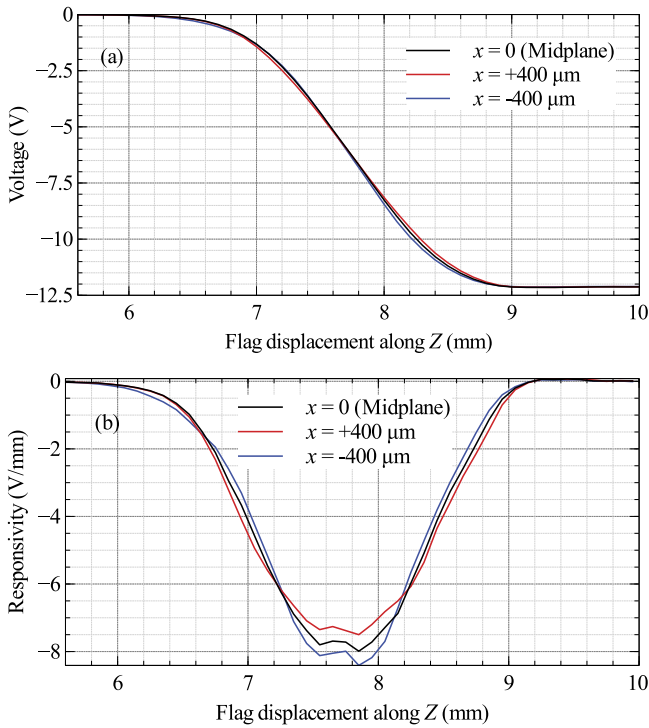


FIG. 7. (a) Calibration and (b) responsivity curves of OSEM #5.

ment by moving the flag with a micrometric translation stage. The first calibration measurement was taken when moving the flag in the z direction in the plane midway ($x = 0$) between the LED and photodiode holders. In order to estimate the error introduced by a deviation of the flag from the midplane while still using the calibration for the nominal position, the calibration was repeated when the flag was set at two nearby planes. For planes at $x = \pm 400 \mu\text{m}$, typical variations of approximately $\pm 4\%$ were observed in the responsivity, measured in units of V/mm , at the nominal position of the flag in z . As a typical example, Fig. 7 shows the calibration and responsivity curves for OSEM #5. When the flag was placed at the midplane $x = 0 \mu\text{m}$, the calibration factor was $-7.51 \text{ V}/\text{mm}$, whereas at planes $x = 400, -400 \mu\text{m}$, the factor differed by 5.2% and 4.1% , respectively. In all cases, the variations were asymmetric

despite being measured at symmetrically opposed planes. In some cases, the asymmetry was more pronounced than in others. This effect is likely produced by a large asymmetry in the light distribution of the LED. The output of the OSEM was also measured when placing the flag in different positions along the y direction and no significant coupling was observed with the movement along the z direction. The noise spectral density of one of the OSEMs was measured to be $0.6 \text{ nm}/\sqrt{\text{Hz}}$ at 1 Hz .

V. DAMPING THE PAYLOAD SUSPENSIONS RESONANCES USING THE OSEMS

The system was placed in a relatively low vacuum of about 3 Pa within one of the vacuum chambers of TAMA300 located at NAOJ in Mitaka. In order to quantify the amount of damping provided by the active system, the quality factors Q of various resonances was measured, first having the feedback system off and later on. Each value of Q was estimated by exciting each mode of the payload with a sinusoidal disturbance at the frequency of interest using the OSEMs and then by estimating the damping time with a least-square fit to the ringdown of the displacement after the excitation had ceased. The value of the quality factor was calculated as $Q = \pi f_0 \tau$, where f_0 is the resonance frequency and τ is the time in which the amplitude decreases by $1/e$.

As an example, let us consider the plot shown in Fig. 8. The thick red line describes the transfer function of the IM measured with the OSEMs mounted on the IRM, from the longitudinal virtual actuator along the optic axis of the main interferometer to its corresponding virtual sensor when noise is injected into the system through the same OSEMs, when the active control system is off. Fig. 9 shows the configuration of the mode with the lower frequency predicted by SUMCOM. The IRM and the BF move together in one direction and the optic, the RM and the IM move together in the opposite direction (mode 17 in Ref. 16). Fig. 8 also shows the simultaneously measured transfer functions in the other degrees of freedom quantifying the coupling with the longitudinal virtual actuator. The transfer function reveals resonances at 0.546 Hz (mode 17 in Ref. 16) and at 1.171 Hz (modes 29 and 31 in Ref. 16). At about 40 Hz , the transfer functions

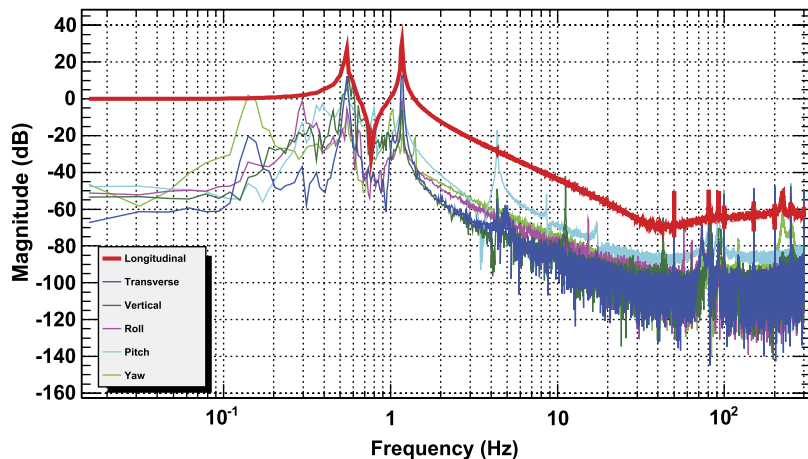


FIG. 8. Transfer functions for the IM without any active damping when the IM is actuated with the longitudinal virtual actuator along the optic axis of the main interferometer. Two resonances are clearly seen at 546 mHz and 1.171 Hz .

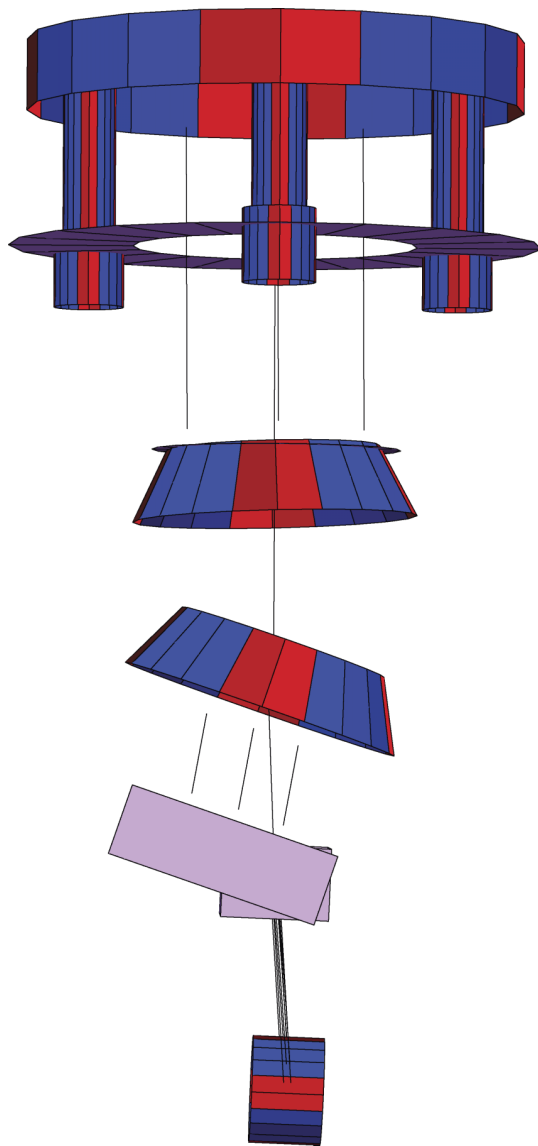


FIG. 9. Graphical representations of oscillation mode #17 generated by SUMCOM.¹⁶

slightly increase and some peaks appear. Such a feature also appears in the transfer functions of the optic. Nevertheless, these features were proved to be electromagnetic coupling since they were also present when the cables of the OSEMs of the RM were disconnected at the OSEMs end and the transfer function measured again. The peaks are mainly hum noise at 50 Hz and at its harmonics and the peaks at 80 Hz and 90 Hz are likely the violin modes of the wires holding the RM, whose lowest mode is in that frequency region.

In order to excite the first resonance, a disturbance was applied at a frequency of 0.542 Hz using the longitudinal actuator in the IM. Fig. 10 shows the displacement measured in pitch after the disturbance had ceased and the control system had been turned on for all degrees of freedom. A model for this behaviour which fits well the data is the function $s = A_1 \exp(-t/\tau) \sin(2\pi f_0 t + \phi) + A_2$, where s is the measured displacement, t is the time, and the rest of the parameters are estimated by the fit. The decay time is $\tau = 5.0$ s, frequency $f_0 = 0.547$ Hz, and $Q = 8.6$.

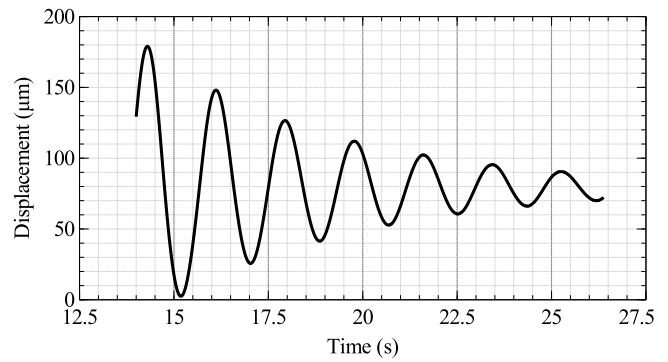


FIG. 10. The oscillation is damped by the active control system.

Fig. 11 shows the measured values of the quality factors with and without control. Numbers are added to facilitate identification and comparison and their definition is given in Ref. 16. In some cases, one single data point describes two modes at neighboring frequencies that are difficult to distinguish.

These measurements refer to an initial stage in which the largest resonances of the system are damped to allow other devices which are not part of the payload take control, namely, geophones on the IP stage and an optical lever monitoring the orientation of the optic from the ground. Besides the OSEMs, the damping also relies on LVDTs (Linear Variable Displacement Transducers) in the GAS filters and on the IP which, all together, should yield an RMS residual motion of the optic of less than approximately 50 μm in the direction of the optic axis and 50 μrad in pitch and yaw.⁶ Analysis of the devices not belonging to the payload goes beyond the scope of this manuscript, nevertheless it is worth pointing out that by employing the optical lever and an external displacement sensor, it was determined that the residual motion achieved was successfully below the requirement.⁶

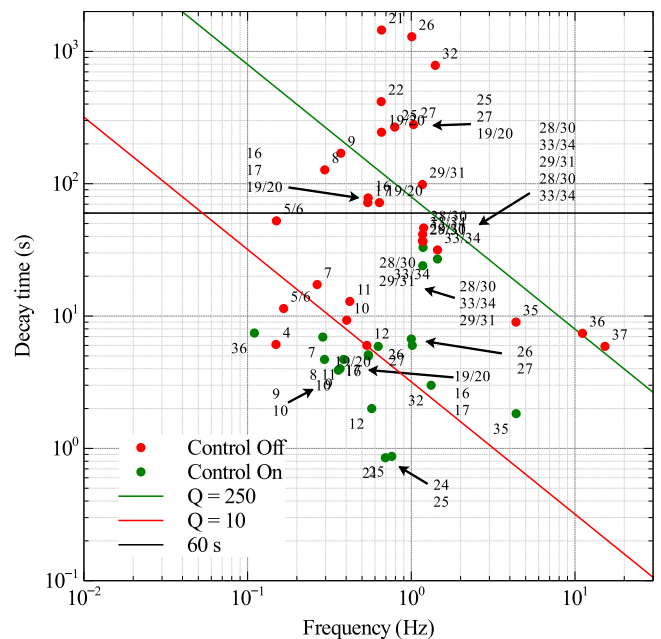


FIG. 11. Quality factors Q of the system when the control system is off and on.

VI. ALIGNMENT CAPABILITIES

In order to assess the alignment range limitations of the payload, the displacement range of the IM was determined. This range depends on the alignment of the OSEMs and on the relative alignment of the IRM with respect to the IM. The measurement was achieved by moving the IM with the coil-magnet actuators of the OSEM by using a sinusoidal signal with a DC offset that increases by steps and later by noting the offset in which the readout of the OSEM revealed a contact between bodies, typically a flag with its OSEM body.

The first step was to set the signals in roll, pitch, and yaw to zero, condition in which the relative displacement between the IM and the IRM was approximately $79\ \mu\text{m}$, $-90\ \mu\text{m}$, and $-10\ \mu\text{m}$ on the longitudinal, transverse, and vertical directions, respectively. The following step was to excite the IM with a sinusoidal signal at 3 Hz with an amplitude of approximately $\pm 2\ \mu\text{m}$ using the virtual sensor corresponding to the degree of freedom under examination. Then the values of the DC offset were changed until the bodies touched each other. Fig. 12(a) shows the free oscillation of the IM when the roll was tested using a small offset value. Fig. 12(b) shows the oscillation once there was physical contact. In this particular case, the maximum DC offset that allows a free oscillation was 5.9 mrad. Before testing the following degree of freedom, the offsets in roll, pitch, and yaw were nulled again. In all the measurements, the active control system was on for all the degrees of freedom which were not tested and the corresponding virtual sensors had residual oscillation amplitudes of about $1\ \mu\text{m}$ full amplitude. Table I shows the results of the measurements.

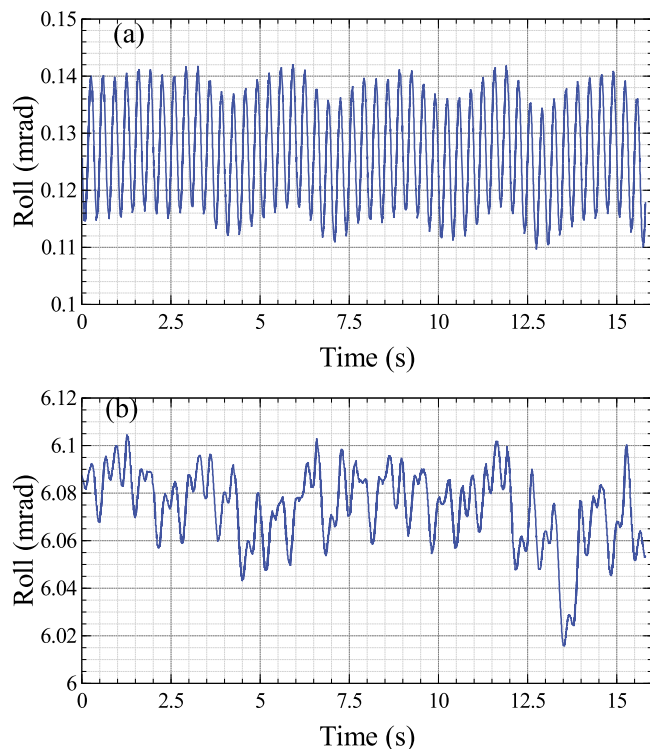


FIG. 12. (a) Oscillation in roll when the IM does not touch the IRM. (b) Once they touch additional oscillation modes appear.

TABLE I. Alignment range of the IM.

DOF	Minimum (mrad)	Maximum (mrad)
Roll	-4.7	5.9
Pitch	-5.0	5.0
Yaw	-1.8	3.5

VII. DISCUSSION

One of the most challenging tasks in the assembly of the current design of the payload is the alignment of the IM with the IRM. The alignment has to be achieved within the tight alignment tolerance of the OSEMs. According to results presented in Sec. IV, in most cases, in order to achieve an error of $\pm 4\%$ in the estimation of the displacement, the flags have to be within $\pm 400\ \mu\text{m}$ from their nominal position. Of course, none of the flags should touch any of the OSEM bodies. Both of these requirements are very challenging to meet given the dimensions and complexity of the IM and IRM. Although the tilt of each OSEM can be adjusted separately, it is very difficult to do this when the system is hanging free, especially for the OSEMs on top of the IRM, where the access is obstructed by cables, cable clamps, and suspension rods, with the additional constraint of a limited gap between the IRM and the BF. Unfortunately, no sideways adjustment of the OSEM was foreseen, which proved to be a problem. For the KAGRA payload, the OSEMs will be mounted on separate holders whose sideways positions can be adjusted once they are mounted on the IRM. This is expected to ease the alignment considerably. In the prototype, the alignment was achieved by tilting the OSEM bodies, strategy which likely introduced additional couplings between different degrees of freedom.

For all the modes whose quality factors were measured with the control system on, $\tau < 50\ \text{s}$ and $Q < 250$. This is already an useful result. In case the lock of the main interferometer is lost due to an unexpected temporary excess of vibrations of the system, it is then easy to acquire it again without having to wait for too long. However, there are other modes which should still be experimentally examined. Especially interesting are the transverse modes of the optic and RM, for which there are no sensors and actuators. These modes are expected to be damped to a certain extent by the OSEM at the IM level and by the magnetic damper depicted in Figs. 1 and 2(a). Unfortunately, in earlier experiments, it was determined that the magnetic damper was not effective enough likely due to the flexibility of the supporting rod and then removed. Nevertheless, this mode is not expected to be an immediate problem in KAGRA due to the large radius of curvature of the mirrors. For the power recycler mirrors, signal recycler mirrors, and beam splitter, an oscillation no bigger than one millimeter will not affect the sensitivity of KAGRA.¹⁷

VIII. CONCLUSIONS AND FUTURE WORK

The functionality of the payload comprises three tasks: holding the optics, its alignment, and the active damping of the resonant modes of the suspension itself. Measurement of the

quality factors Q and damping times τ of resonant oscillations with the active control system on yielded typical values of $Q < 250$ and $\tau < 50$ s. The angular alignment range of the payload, in which the IM can move without touching the IRM, was measured to be $(-4.7, 5.9)$ mrad in roll, $(-5.0, 5.0)$ mrad in pitch, and $(-1.8, 3.5)$ mrad in yaw.

The prototype experiment also aimed to test the suitability of the hardware to achieve a successful coarse alignment. During the assembly, it became clear that the alignment of the IRM hanging rigidly from the BF was very challenging. Any tilt of the BF would not only tilt the IRM, but it would also displace it sideways, moving the flags within the OSEMs too much and compromising the alignment. The problem is expected to lessen in the KAGRA payload by mounting the OSEMs in individual holders than can slide sideways once mounted on the IRM.

Future work includes the assembly of five payloads at Kamioka for iKAGRA (Initial KAGRA). Installation and commissioning will require troubleshooting of the modified version of the payload.

ACKNOWLEDGMENTS

This work was supported by MEXT, JSPS Leading-edge Research Infrastructure Program, JSPS Grant-in-Aid for Specially Promoted Research No. 26000005, MEXT Grant-in-Aid for Scientific Research on Innovative Areas No. 24103005, JSPS Core-to-Core Program, A. Advanced Research Networks, and the joint research program of the Institute for Cosmic Ray Research, University of Tokyo.

We highly appreciate the assistance given by the Advanced Technology Center of the NAOJ during the assembly of the payload prototype.

¹K. Somiya, *Classical Quantum Gravity* **29**, 124007 (2012).

²P. R. Saulson, *Phys. Rev. D* **42**, 2437 (1990).

³M. G. Beker, G. Cella, R. DeSalvo, M. Doets, H. Grote, J. Harms, E. Hennes, V. Mandic, D. S. Rabeling, J. F. J. Brand, and C. M. Leeuwen, *Gen. Relativ. Gravitation* **43**, 623 (2010).

⁴A. Bernardini, E. Majorana, P. Puppo, P. Rapagnani, F. Ricci, and G. Testi, *Rev. Sci. Instrum.* **70** (1999).

⁵L. Carbone, S. M. Aston, R. M. Cutler, A. Freise, J. Greenhalgh, J. Heefner, D. Hoyland, N. A. Lockerbie, D. Lodhia, N. A. Robertson, C. C. Speake, K. A. Strain, and A. Vecchio, *Classical Quantum Gravity* **29**, 115005 (2012).

⁶T. Sekiguchi, "A study of low frequency vibration isolation system for large scale gravitational wave detectors," Ph.D. thesis, University of Tokyo, 2016.

⁷T. Sekiguchi *et al.*, "Demonstration of active vibration control of the KAGRA seismic attenuation system" (unpublished).

⁸A. Takamori, P. Raffai, S. Márka, R. DeSalvo, V. Sannibale, H. Tariq, A. Bertolini, G. Cella, N. Viboud, K. Numata, R. Takahashi, and M. Fukushima, *Nucl. Instrum. Methods Phys. Res., Sect. A* **582**, 683 (2007).

⁹R. DeSalvo, A. DiVirgilio, A. Errico, F. Guotong, I. Ferrante, F. Frasconi, A. Gaddi, A. Gennai, G. Gennaro, A. Giazotto, L. Holloway, G. Losurdo, M. Maggiore, S. Mancini, M. Mazzoni, F. Palla, P. H. Bao, F. Paoletti, A. Pasqualetti, R. Passaquieti, D. Passuello, R. Poggiani, P. Popolizio, F. Raffaelli, D. Righetti, R. Ruberti, V. Rubino, P. Ruggi, R. Stanga, R. Taddei, R. Valentini, A. Vicere, J. Winterflood, Z. Zhou, M. Bernardini, A. Bozzi, S. Braccini, C. Bradaschia, C. Casciano, G. Cella, A. Ciampa, G. Curci, E. D'Ambrosio, V. Dattilo, G. DeCarolus, and A. Delapierre, *Nucl. Instrum. Methods Phys. Res., Sect. A* **420**, 316 (1999).

¹⁰F. E. Peña Arellano, Alignment capabilities of the room temperature payload, <http://gwdoc.icrr.u-tokyo.ac.jp/cgi-bin/DocDB/ShowDocument?docid=4246>, 2015.

¹¹T. Sekiguchi, SUMCOM, <http://gwdoc.icrr.u-tokyo.ac.jp/cgi-bin/DocDB/ShowDocument?docid=3729>, 2015.

¹²T. Sekiguchi, "Modeling and simulation of vibration isolation system for large-scale cryogenic gravitational-wave telescope (LCGT)," Master's thesis (University of Tokyo, 2012).

¹³Y. Fujii, T. Sekiguchi, R. Takahashi, Y. Aso, M. Barton, F. E. Peña Arellano, A. Shoda, T. Akutsu, O. Miyakawa, M. Kamiizumi, H. Ishisaki, D. Tatsumi, N. Hirata, K. Hayama, K. Okutomi, T. Miyamoto, H. Ishizuka, R. DeSalvo, and R. Flaminio, Proceedings of the 11th Amaldi Conference, 2015.

¹⁴M. G. Beker, "Low-frequency sensitivity of next generation gravitational wave detectors," Ph.D. thesis, Vrije Universiteit, 2013.

¹⁵M. Barton, Osem coil/magnet/flag calculation, <http://gwdoc.icrr.u-tokyo.ac.jp/cgi-bin/DocDB/ShowDocument?docid=3239>, 2015.

¹⁶Y. Fujii, Quality factor measurement, <http://gwdoc.icrr.u-tokyo.ac.jp/cgi-bin/DocDB/ShowDocument?docid=4244>, 2015.

¹⁷Y. Aso, Y. Michimura, K. Somiya, M. Ando, O. Miyakawa, T. Sekiguchi, D. Tatsumi, H. Yamamoto, and KAGRA Collaboration, *Phys. Rev. D* **88**, 043007 (2013).